Mirror twin boundaries in $MoSe_2$ monolayers as one dimensional nanotemplates for selective water adsorption

Li, J.; Joseph, T.; Ghorbani Asl, M.; Kolekar, S.; Krasheninnikov, A.; Batzill, M.;

Originally published:

December 2020

Nanoscale 13(2021)2, 1038-1047

DOI: https://doi.org/10.1039/D0NR08345C

Mirror twin boundaries in $MoSe_2$ monolayers as one dimensional nanotemplates for selective water adsorption

Jingfeng Li,[1,#] Thomas Joseph,[2,#] Mahdi Ghorbani-Asl,[2] Sadhu Kolekar,[1] Arkady V. Krasheninnikov,[2,3] Matthias Batzill[1,*]

[1] Department of Physics, University of South Florida, Tampa, FL 33647, USA

[2] Helmholtz-Zentrum Dresden-Rossendorf, Institute of Ion Beam Physics and Materials Research, 01328 Dresden, Germany

[3] Department of Applied Physics, Aalto University, P.O. Box 11100, 00076 Aalto, Finland

[#] authors contributed equally

[*] Corresponding author: Matthias Batzill; e-mail: mbatzill@usf.edu

Abstract:

Water adsorption on transition metal dichalcogenides and other 2D materials is generally governed by weak van der Waals interactions. This results in a hydrophobic character of the basal planes, and defects may play a significant role in water adsorption and water cluster nucleation. However, there is a lack of detailed experimental investigations on water adsorption on defective 2D materials. Here, by combining low-temperature scanning tunneling microscopy (STM) experiments and density functional theory (DFT) calculations, we study in that context the well-defined mirror twin boundary (MTB) networks separating mirror-grains in 2D $MoSe_2$. These MTBs are dangling bond-free extended crystal modifications with metallic electronic states embedded in the 2D semiconducting matrix of $MoSe_2$. Our DFT calculations indicate that molecular water also interacts similarly weak with these MTBs as with the defect-free basal plane of $MoSe_2$. However, in low temperature STM experiments, nanoscopic water structures are observed that selectively decorate the MTB network. This localized adsorption of water is facilitated by functionalization of the MTBs by hydroxyls formed by dissociated water. Hydroxyls may form by dissociating of water at undercoordinated defects or adsorbing of radicals from the gas phase in the UHV chamber. Our DFT analysis indicates that the metallic MTBs adsorb these radicals much stronger than on the basal plane due to charge transfer from the metallic states into the molecular orbitals of the OH groups. Once the MTBs are functionalized with hydroxyls, molecular water can attach to them, forming water channels along the MTBs. This study demonstrates the role metallic defect states play in the adsorption

of water even in the absence of unsaturated bonds that have been so far considered to be crucial for adsorption of hydroxyls or water.

Key words: van der Waals materials; water adsorption; defect engineering; hydroxylation; metallic defect states; molecular scale adsorption template.

TOC- figure:

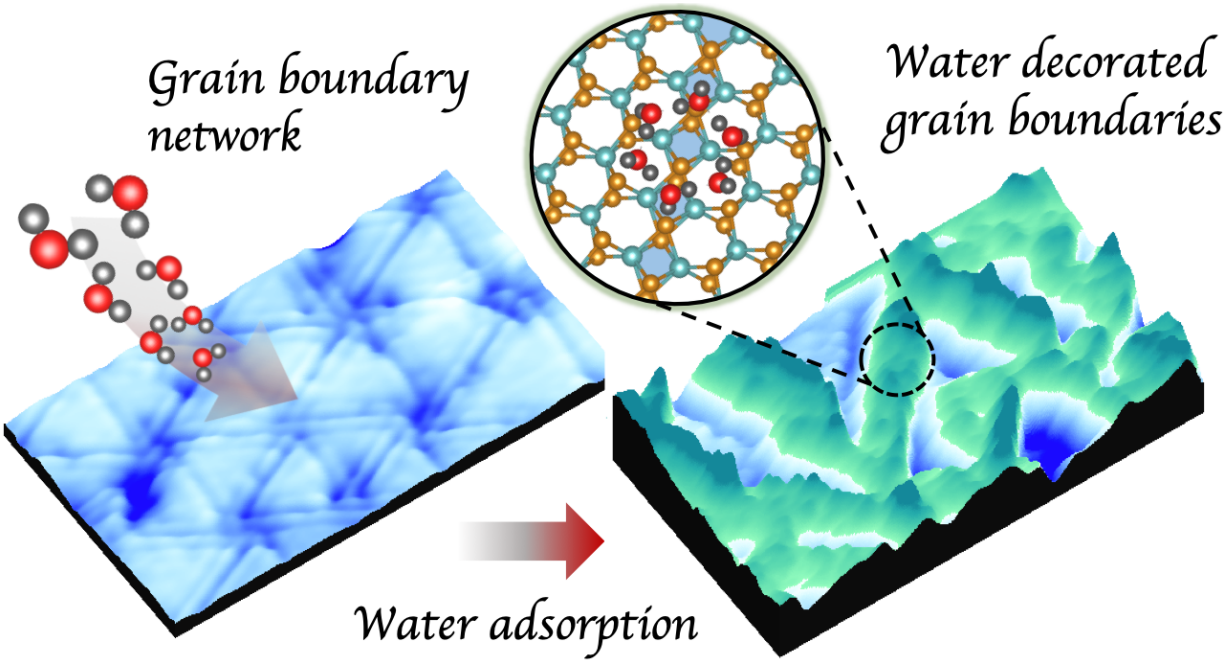

Introduction

Water adsorption on surfaces has extensively been investigated due to its prominent role in many environmentally and technologically important phenomena, ranging from water condensation on aerosol particles and corrosion to chemical transformations in aqueous solutions. Specifically, vacuum surface science investigations have provided fundamental insights into water adsorption on single crystal surfaces,[1,2,3] and understanding of the ordering of water monolayers on surfaces has been gained from a combination of scanning tunneling microscopy (STM) experiments and density functional theory (DFT) calculations.[4,5,6,7,8] The monolayer structure is found to be defined by the delicate balance between the interaction of water molecules with the substrate and the neighboring water molecules, which may be altered by cooperative effects, i.e. the substrate interactions can also modify the molecule-molecule interactions.[9,10] In addition to molecular adsorption, dissociation of water on surfaces and the formation of hydroxyl (OH)-groups bound to the substrate has been shown to be important on some metal as well as oxide surfaces.[11,12,13] Such OH groups can act as 'anchors' for additional water molecules to adhere to and can transform hydrophobic surfaces to hydrophilic ones.[14,15] On oxide surfaces such OH groups often form at defects that then can be nucleation sites for water clusters. On FeO-monolayers on Pt(111), for instance, an amorphous water monolayer was observed, while hydrogenation of specific sites in the iron oxide moiré structure on Pt(111) enabled the modification of water adsorption into nanoclusters around these localized hydroxyl-groups.[16] This demonstrates that directed modification of surfaces with hydroxyls can result in nano-structured water layers.

On van der Waals (vdW) materials the lack of unsaturated bonds at surfaces results in very weak water-substrate interactions,[17,18,19] and water adsorption in vacuum is only possible at low temperatures. Initial water nucleation is generally observed as ring-structures in water-pentamers or hexamers.[5] At extended coverage, ice-like structures are predicted to form.[20] For graphene-[21] or *h*-BN[22] -monolayers on metal substrates regular moiré structures may form with strong electrostatic modulations of the surface, and this may lead to patterning of the material. As a consequence, localized water adsorption at preferential sites of the moiré superstructure has been observed, giving rise to the formation of nano-water islands.

In this context, we investigate here water adsorption on $MoSe_2$, the typical two-dimensional (2D) transition metal dichalcogenide (TMD), and one of the most technologically important 2D material. The lack of dangling bonds on TMDs gives, like on other 2D materials, rise to weak adsorption.[18,19, 23] TMDs have been suggested as potential materials for electrocatalytic applications in aqueous solutions and their (electro)catalytic properties, specifically for hydrogen evolution reaction (HER) are generally attributed to defects, specifically undercoordinated atoms

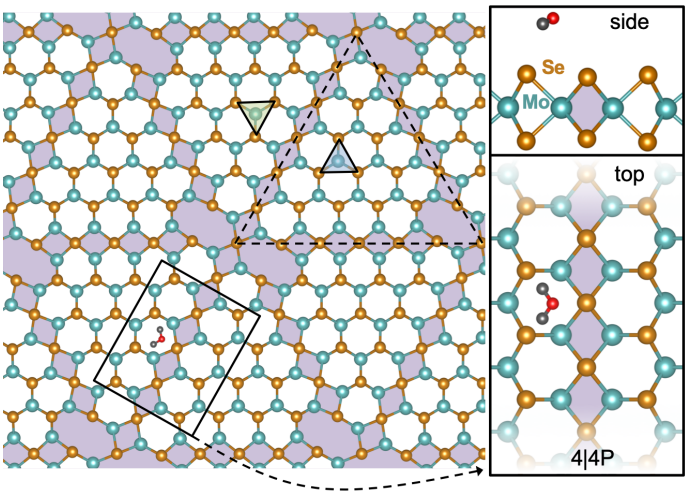

Figure 1: *Schematic representation of water adsorption on the 4|4P MTB network in $MoSe_2$ monolayer. Note that the spacing between the vertices where the MTBs meet is much smaller than in the experiment. Correspondingly, MTB density is much higher. The defect free TMD grains are shown on a white background with the grain orientation indicated by the triangles, illustrating the mirror domains. The domain boundaries and vertices are shown on gray background.*

at the edges or chalcogen vacancies.[24,25,26] Other defects such as grain boundaries may also exhibit special chemical activity,[27] but because of the low density of these defects, their catalytic properties have been scarcely studied. A special kind of grain boundaries with increased electrocatalytic activity[28] are mirror twin boundaries (MTBs) that are formed between two grains rotated by 60° as shown in **Fig. 1**. While different atomic configurations of these grain boundaries can be obtained in dichalcogenides, the common configuration in $MoSe_2$ is the metal rich structure, which is referred to as 4|4P.[29, 30, 31] It has been demonstrated that this configuration can be generated in $MoSe_2$ or $MoTe_2$ by incorporation of excess Mo-atoms, causing the formation of triangular MTB loops.[32] Therefore, incorporation of excess Mo is a potential approach for modifying sheets of $MoSe_2$ basal planes with MTB networks and consequently

altering their properties and potentially enhancing chemical functionalities. In contrast to other nanopatterned 2D surfaces that have been shown to possess modified reactivity,[21,22,33] MTB networks in TMDs, schematically illustrated in **Fig. 1**, are intrinsic crystal-modifications and do not require artificial growth on a metal substrate, but can be obtained also in free-standing TMD sheets. Thus, these material modifications are of potential relevance for practical applications. Moreover, it has been demonstrated that MTBs are metallic[34,35,36] and thus could also assist charge transport in the semiconducting TMD-based electrocatalysts. The interaction of MTB modified TMDs with water is of importance for applications in aqueous solutions and maybe considered as model systems to study water interactions with metallic defect states. While most defect structures exhibit higher chemical activities due to the formation of unsaturated bonds, MTBs are perfect one-dimensional crystal structures, without broken bonds and thus the surface may still be considered as a vdW surface that is only electronically modulated by the metallic MTBs. Using DFT calculations, we show that due to the lack of unsaturated bonds, water molecules interact very weakly with these MTBs and the adsorption is barely modified as compared to the defect free basal plane. However, the MTBs adsorb OH-groups much stronger than the basal plane of $MoSe_2$. This leads to a functionalization of the MTBs with OH-groups that subsequently can anchor water molecules and form amorphous water networks that decorate the OH-functionalized MTBs. These experimentally observed water networks are a direct verification of the chemical functionality of MTBs to induce nanostructured adsorption.

Results and Discussions

Monolayer islands of $MoSe_2$ were grown on highly oriented pyrolytic graphite (HOPG) substrates by molecular beam epitaxy. The HOPG substrate allows vdW epitaxy, i.e. ensures weak interaction between the $MoSe_2$ and the substrate, but its good conductivity allows STM investigations at low temperatures, needed for the adsorption of water in vacuum. It has been reported that MBE growth of $MoSe_2$ on HOPG or other van der Waals substrates yields samples that exhibit MTB networks due to the incorporation of excess Mo into the crystal structure during growth.[35,37]

Sample characterization by STM: STM images of the as grown sample are presented in **Fig. 2 (a).** The large-scale image shows the edges of a $MoSe_2$ monolayer island, with only small bilayer

regions. Note that under the imaging conditions in Fig. 2(a) (-1V, 50 pA) the electronic contrast of the MTBs make them appear with a large corrugation and an apparent height of ~ 0.2 nm above the basal plane of $MoSe_2$. The edges of the $MoSe_2$ island appear similarly bright as the MTBs, indicating that they also have a metallic character. The imaging contrast is strongly bias voltage dependent, as illustrated in **Fig. 2 (b)** and **(c)**. At negative bias voltages (tunneling from filled states in the sample) the MTBs appear as bright (double) lines. This double line feature in STM of the MTBs has been confirmed by simulated STM images.[32] At positive bias voltages (tunneling into empty states in the sample) the contrast between the basal plane and the MTBs is less pronounced, **Fig. 2(c)**. This contrast in STM stems from the metallic character of the MTBs and the fact that their charge neutrality level lies much closer to the conduction band minimum (CBM) than the valence band maximum (VBM), i.e. $MoSe_2$ with MTBs is strongly n-type due to the pinning of the Fermi-level to the MTB-induced defect states. In this case, tunneling at negative bias voltages as large as -1V is still withing the band gap of MoSe2 and thus giving rise to the very strong electronic contrast of the MTBs. For empty states, at positive voltages, we already tunnel into the conduction band of $MoSe_2$ for the strong n-type material and thus causing less contrast variation between MTBs and the pristine $MoSe_2$. At low temperatures, the MTBs exhibit a modulation along the MTBs of 3 times their lattice constant. This has been suggested to be a consequence of the strictly 1D metallic nature and may be either due to a Peierls' instability,[34, 38] or a result of strong-correlations, as described within the framework of the Tomonaga-Luttinger quantum liquid in the 1D electron system.[36] At low temperatures, we can also identify the moiré structure in the extended regions of the pristine $MoSe_2$ induced by the differences in the lattice constant of the HOPG substrate and $MoSe_2$,[37] as shown in **Fig. 2(d).** Surprisingly, the moiré structure is not well resolved if we image the surface at room temperature. On the other hand, room temperature imaging allows imaging with lower bias voltage, presumably because of better conductivity of the sample. At the lower bias voltage, the atomic structure of the MTBs is resolved better as seen in **Fig. 2(e),** which shows clear atomic corrugation along the MTBs. Surprisingly, some of the MTBs still show a periodicity of three times the lattice constant even at room temperature, with every third atom appearing brighter, as indicated in the line scan in **Fig. 2(e).**

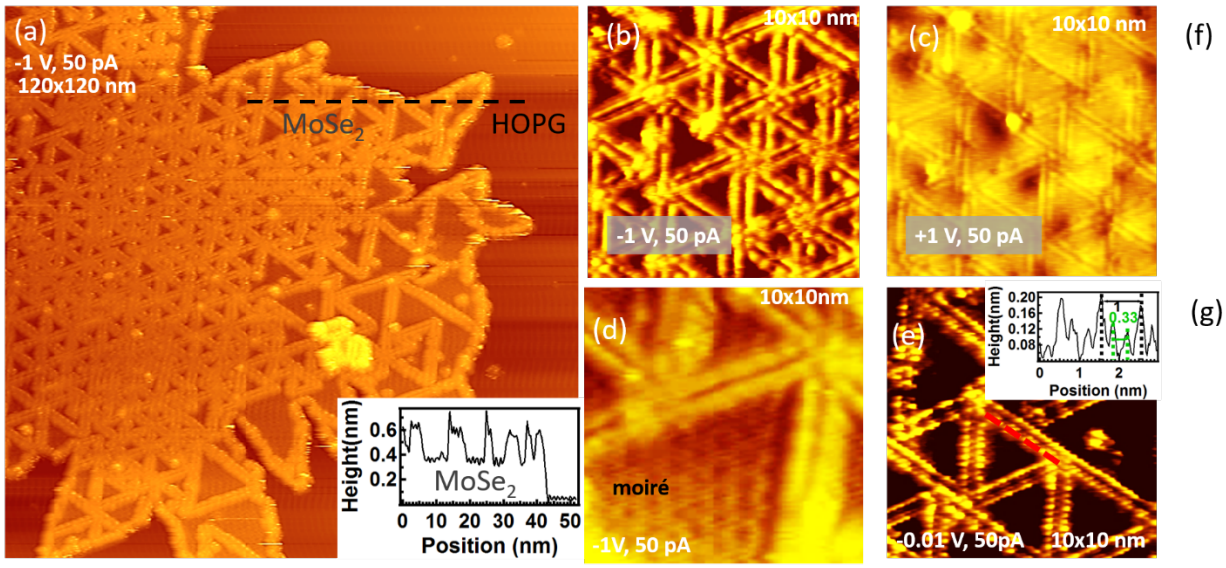

Figure 2: *STM characterization of $MoSe_2$ monolayers grown on HOPG substrate. (a) Large scale image showing a partial $MoSe_2$ island and HOPG substrate area. The $MoSe_2$ island is covered with a dense MTB network. Under the imaging conditions in (a) the metallic MTBs exhibit a very strong electronic contrast with an apparent height of ~ 0.2 nm. The inset shows a line-scan, indicated by the dashed line in the STM image, showing both the height of the $MoSe_2$ basal plane of ~ 0.35 nm with respect to the HOPG substrate and the apparent height of the MTBs. The bias dependent image contrast is highlighted in (b) and (c), which show the same image area with 1V negative (filled states) and positive (empty states) bias. (d) shows the moiré pattern of $MoSe_2$ basal plane on HOPG substrate in between of MTB networks. The periodic distortion of the metallic MTBs with 3 times the lattice constant is shown in (e). The line scan along one MTB is shown in the inset, with the atomic corrugation of 0.33 nm and the superstructure of 1.0 nm indicated.*

MTBs form by nucleation and growth of triangular MTB-loops,[32] with the inside of the loops exhibiting a mirror domain relative to the outside of the loop. These loops grow until they are impeded by interaction with the $MoSe_2$-island edge or by interaction with other MTBs. Thus, the MTB network is a consequence of merging of MTB-loops. In a second stage, new loops may nucleate within existing loops and thus, especially in the center of the growing $MoSe_2$ islands, denser MTB-networks are observed that are surrounded by larger MTB triangles. The MTBs are often joined at their vertices, and while the MTBs themselves are 1D lattice modifications without dangling bonds, the vertices exhibit more complex morphologies with unsaturated bonds that

could affect adsorption. For instance, it has been shown that some of these vertices are the preferred nucleation sites for gold clusters.[35] STM images reveal different configurations at which the MTBs meet, with various offsets between the line defects at the vertices. Unfortunately, the convolution of electronic and topographical contrast in STM makes a detailed determination of the atom positions in the vertices challenging, although previous attempts have been made using non-contact AFM.39 Because of the unknown detailed atomic structure and composition, as well as the presence of several different configurations of these vertices, we are not discussing these further in this manuscript, apart from pointing out that they potentially could facilitate the dissociation of water. The focus of this manuscript is on the well-defined MTBs as a model of metallic crystal modification with a vdW (no dangling bonds) surface termination.

Water adsorption studied by STM: Water is dosed through a precision leak valve and a stainless-steel tube directed onto the sample mounted in the STM and cooled to ~20 K. The opening of the leak valve was detected by an increase of the residual water pressure in the vacuum chamber background using a quadrupole mass spectrometer. The precise exposure of water to the sample could not be measured and thus the sticking probability of water on the sample is unknown. From the increase in the background pressure and the exposure time we can estimate a lower limit of the exposure and we give these values as the nominal exposure in Langmuir (1L = 10^{-6} Torr/sec). The true water exposure through the directed dosing line is expected to be significantly larger. As we discuss below, even this large exposure only leads to sub-monolayer coverage, indicating a very low adsorption on the surface even at this low temperature. High exposures also make it likely that dissociated water may adsorb, either from small fractions present in the beam or from water dissociated in the vacuum chamber on e.g. filaments of the ion gauge or mass-spectrometer.

Imaging of weakly bound water on the surface is challenging with STM due to tip sample interactions. In our studies we found that individual water penta- or hexamers can be readily imaged under filled state imaging condition. For higher coverage this leads, however, to unstable imaging. Empty state imaging with low tunneling current (i.e. large tip-sample separation) are the only conditions to image the adsorbed water. Filled state images (-1 V; 50 pA) or large positive bias voltage (+6 V; 50 pA) allows to remove the water off the surface and this enables to image

the underlying structure in subsequent imaging of the cleaned region. In the following we investigate STM images of samples with increasing water exposure in order to reveal the preferential adsorption sites and the evolution of the water layer with increasing water coverage. **Fig. 3** shows filled state STM images for low water exposures. Under these conditions small water clusters form at the surface, that exhibit a ring structure in STM. On rare occasions a substructure is observed that reveals individual protrusions along the ring, which may be associated with individual water molecules. The inset in **Fig. 3(b)** shows such a case with 5 protrusions. The fact that we generally cannot resolve individual water molecules suggest that they are mobile or fluctuate on a timescale faster than the several seconds it takes to record an STM image. The water clusters can be clearly distinguished from other features on the sample by their apparent height in STM images. Line-scans shown in **Fig. 3** illustrates the apparent height of the MTBs above the $MoSe_2$ basal plane of 0.11 nm, indicated as the red dashed line in **Fig. 3.** While there are other bright protrusions, e.g. at MTB vertices, these are less pronounced than the height of the water clusters that are ~ 0.07 nm taller than the MTBs. This height of the water clusters is indicated as the green dashed line in the line scans shown in **Fig. 3.** Thus, the imaging height enables us to unambiguously identify the water clusters. In **Fig. 3(b)** the water clusters are indicated by white arrows. Importantly, all these small water clusters are on or adjacent to MTBs and initially have a tendency to be close to the vertices of the MTBs. In this low dosage regime, the number of water clusters increases with the dosage time. With increasing water exposure, the water rings eventually get too close to maintain their individual ring-character. The water appears disorganized or noisy in these images, indicating amorphous water as previously reported for water layers on FeO surfaces modified by hydroxyl groups.[16] The noisiness of the images is attributed to mobility or rotation of the water molecules even at 20 K. Still, water is only imaged along the MTBs and their vertices, no water clusters on the basal planes between the MTBs are observed.

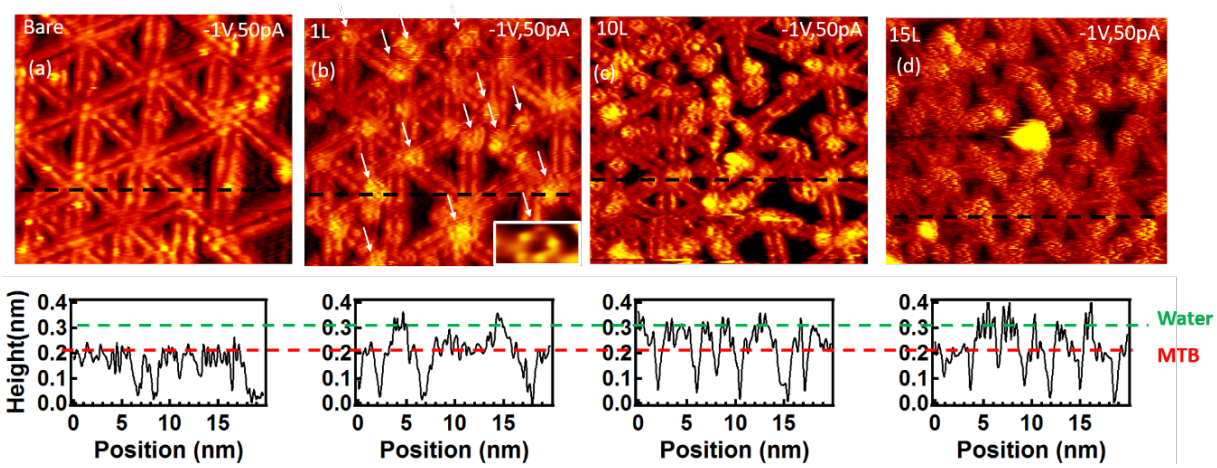

Figure 3: *STM images of water clusters on MTBs for low water exposures. All STM images are 20x18nm and the samples were exposed with increasing amount of water, with nominal exposures of 0L, 1L, 10L, and 15L for (a) –(d). Water clusters are identified by the image height. The water clusters are imaged 0.1 nm above the height of the MTBs, as illustrated by the red and green dashed lines in the line scans.*

With increasing water exposure, water is more clearly imaged under empty state imaging conditions at which the clean MTBs have a less pronounced contrast (see **Fig. 2 (c)**). In **Fig. 4 (a)** a region of the surface is shown where the entire MTB network is covered with water. The imaging conditions are equivalent to those shown in **Fig. 2 (c)** for the bare surface and thus the strong corrugation of the surface is due to the decoration of the MTBs with water. This can be confirmed by imaging part of the surface at negative voltage (-1 V , 50 pA). This causes water to be swept away with the tip and exposes the bare surface. Subsequent imaging of a larger area shows both the MTB network and the water decorated MTBs (shown in **Fig. 4 (b**)), demonstrating that the enhanced contrast is due to water adsorption on the MTBs. While in these small-scale images the decoration of the MTB network is revealed, on large scale images a different structure is observed. The $MoSe_2$ islands are covered by water 'droplets' that increase in size with increasing water exposure, as shown in **Fig. 4(c),** while the HOPG substrate appears to be clear of any water adsorption. On the $MoSe_2$ islands, the water drops can be again swept away with the STM tip and thus expose the clean substrate to demonstrate that these drops are weakly bound adsorbates. This is shown in **Fig. 4(d).** Thus, the water adsorption on MTB-modified $MoSe_2$

forms a hierarchical structure of 2D-water droplets and a water network structure within these drops formed by decorating the MTBs.

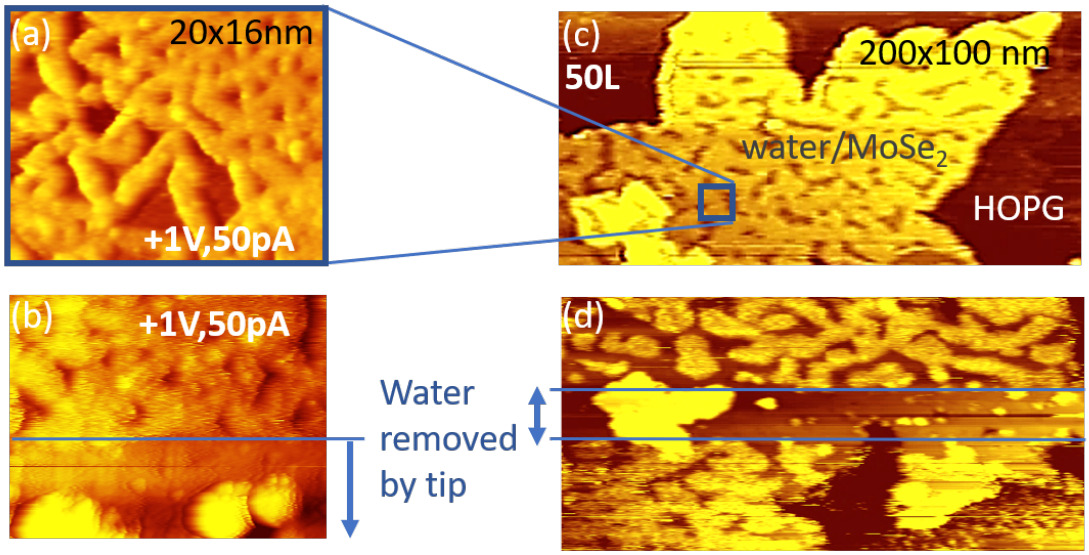

Figure 4: *STM images of water adsorption on $MoSe_2$ for large water exposure (nominal 50 L). water decorating the MTB network imaged with positive bias voltage is shown in (a). Water may be removed from the surface by imaging with negative voltage and this enables to clear part of the surface of water and thus directly compare surface with and without water. A surface partially cleared of water is shown in (b). On large scale images, shown in (c), it is apparent that initially water does not uniformly cover all the MTBs, but an additional hierarchical structure is formed with MTBs only decorated in tens of nanometer wide water islands. These water islands can be again be removed with the STM tip at negative bias voltages as demonstrated in (d).*

The STM data illustrate that water adsorption even at 20 K is selective at MTBs only, while the basal planes remain free of water. Given the high exposure required for water to adsorb suggests an inefficient process. To gain additional insight in the adsorption and the differences between adsorption on the basal plane versus adsorption on MTBs we conducted detailed *ab initio* claculations.

DFT analysis of water adsorption: In order to get microscopic insight into the interaction of water molecules with pristine $MoSe_2$ sheets and those with MTBs, we carried out extensive first-principles calculations within the framework of the spin-polarized DFT, as described in methods

section. The adsorption energy E_{ads} (positively defined) of water molecules was evaluated, along with the formation energy E_f of water clusters. The latter was defined as a difference between the energy of $MoSe_2$ and isolated water molecules in vacuum and the total energy of $MoSe_2$ with the adsorbed water molecules, and normalized by the number of water molecules.

The adsorption of water molecules onto pristine basal planes was investigated first. The full optimization of the geometry of the system using Grimme corrections gave adsorption energy of E_{ads}= 0.18 eV. The lowest energy position of water molecules on top of the basal plane is depicted in **Fig. 5(a).** Calculations with a more accurate TS exchange-correlation functional gave E_{ads}= 0.15 eV. These values are consistent with the results of water adsorption calculations for MoS_2 (0.15 eV),40 as well as on metal (0.1 – 0.4 eV)41 and FeO[16] surfaces. E_f for water rings (pentamer and hexamers) on top of $MoSe_2$ was found to be 0.47 eV per water molecule, **Fig. 5(d),** which is a sum of the energies corresponding to the interaction between the molecules (0.37 eV per H_2O in the isolated system) and adsorption energy, which is less in this case than that for the isolated molecule, as all water molecules in the ring cannot occupy the preferred positions in terms of the vdW interaction. The interaction energy between the molecules in the hexamer is in line with the previously reported value (0.49 eV).[10]

The calculations for water molecules on top of an MTB gave similar results, the adsorption energy was found to be higher (adsorption is energetically more favorable) by ~0.015 eV only, which could hardly explain the experimental observations of water clustering on top of MTBs. As MTBs have metallic states at the Fermi level, so that the additional charge should be localized in these structures, we also investigated the possible effects of doping on the adsorption energy. We found that adding or removing one electron per six unit cells in the MTB has little effect on the adsorption, E_{ads} changes by about 0.01 eV per molecule, and thus could not explain the preferred adsorption either.

As an alternative scenario, we considered the interaction of water molecules with hydroxyl groups, **Fig. 5(b,c)**, which can appear on the surface due to water splitting, as discussed in Ref.[16], or through adsorption of water radicals from the gas phase. We found that adsorption energy of the groups, which is naturally considerably stronger than that for water molecules, as it is of the covalent nature, depends on the position of the group with regard to the MTB. The change in E_{ads}

is about 0.7 eV, **Fig. 5(e),** which makes the adsorption of OH groups on MTB strongly preferable. The increase in E_{ads} is associated with the charge transfer of the electrons localized in the MTB into the empty orbitals of the OH group, **Fig. 5(e),** which are below the Fermi level in the system, as the electronic structure analysis, **Fig. 5(f),** point out. The increase in E_{ads} is associated with the charge transfer of the electrons localized in the MTB into the empty orbitals of the OH groups, **Fig. 5(e)**, which are below the Fermi level in the system, as the analysis of the electronic structure of $MoSe_2$ with MTB and isolated OH group, as **Fig. 5(f)**, points out. We note that the energy diagrams of the isolated systems presented in **Fig. 5(f)** can be used only for getting insights into the qualitative behavior upon radical adsorption, as the amount of the transferred charge is governed by a delicate balance between the changes in the spatial distribution of the electron density and thus electronic state population, followed by the changes in the electronic structure of the combined system, and Coulombic interactions, so that it cannot be estimated from a simple diagram presenting the electronic structures of the isolated systems. Moreover, the position of the levels may not be reliably reproduced by DFT at the PBE/GGA level, but more accurate calculations (RPI or with hybrid functionals) are computationally too expensive for the large supercells required in the system studied here. The actual values of the transferred charge may also depend on the method used to assess it, that is the Bader or 'geometrical' approaches (for an illustration, see, e.g. ref.42).

The interaction of water molecules with the hydroxyl group is much stronger than the adsorption of water on the pristine basal plane of $MoSe_2$ or on MTB, as the bond is of hydrogen rather than vdW type. When further molecules are added, the enhanced interaction with the OH-group, is however, accompanied by a drop in the vdW energy, because the water molecules are not in the optimal position with regard to the basal plane, as illustrated in the right panel in **Fig. 5(c).** Nevertheless, formation of water clusters (at least up to 6 molecules) attached to OH groups is favorable, es evident from **Fig. 5(d),** with a difference of about 0.06 eV per water molecule. The competition between hydrogen and vdW bonding may also explain why large clusters were not observed in the experiments.

Having analyzed the energetics and geometry of the adsorbed OH species, we also studied the energetics of hydrogen atoms on the pristine $MoSe_2$ and in the MTB area. We found that there

are two metastable positions of H atom: as an adatom or an interstitial within the Mo plane, as reported previously for $MoTe_2$, [28] with the energy of the interstitial position being lower by 0.6 eV. Moreover, in line with the behavior in $MoTe_2$, the energy of the H interstitial is lower by 0.15 eV when it is next to the MTB. Thus, the total energy gain when a water molecule is split at the MTB is about 0.7 + 0.15 = 0.85 eV, with the former value representing the gain in E_{ads} for the OH group. It should be pointed out, though, that the energy required to split the molecule at the MTB is overall high (about 2.4 eV), considerably larger than that for vacancies (0.8 eV, according to our calculations), indicating that the latter should be catalytically more active. Similar results have been obtained for other TMDs, e.g., MoS_2, where water splitting is more efficient at structures having undercoordinated atoms/dangling bonds, such as vacancies [43,44,45] or edges.[46,47,48] The vertices at MTB cross sections may have a higher water splitting capacity, but we have not studied them as their precise atomic structure is unknown.

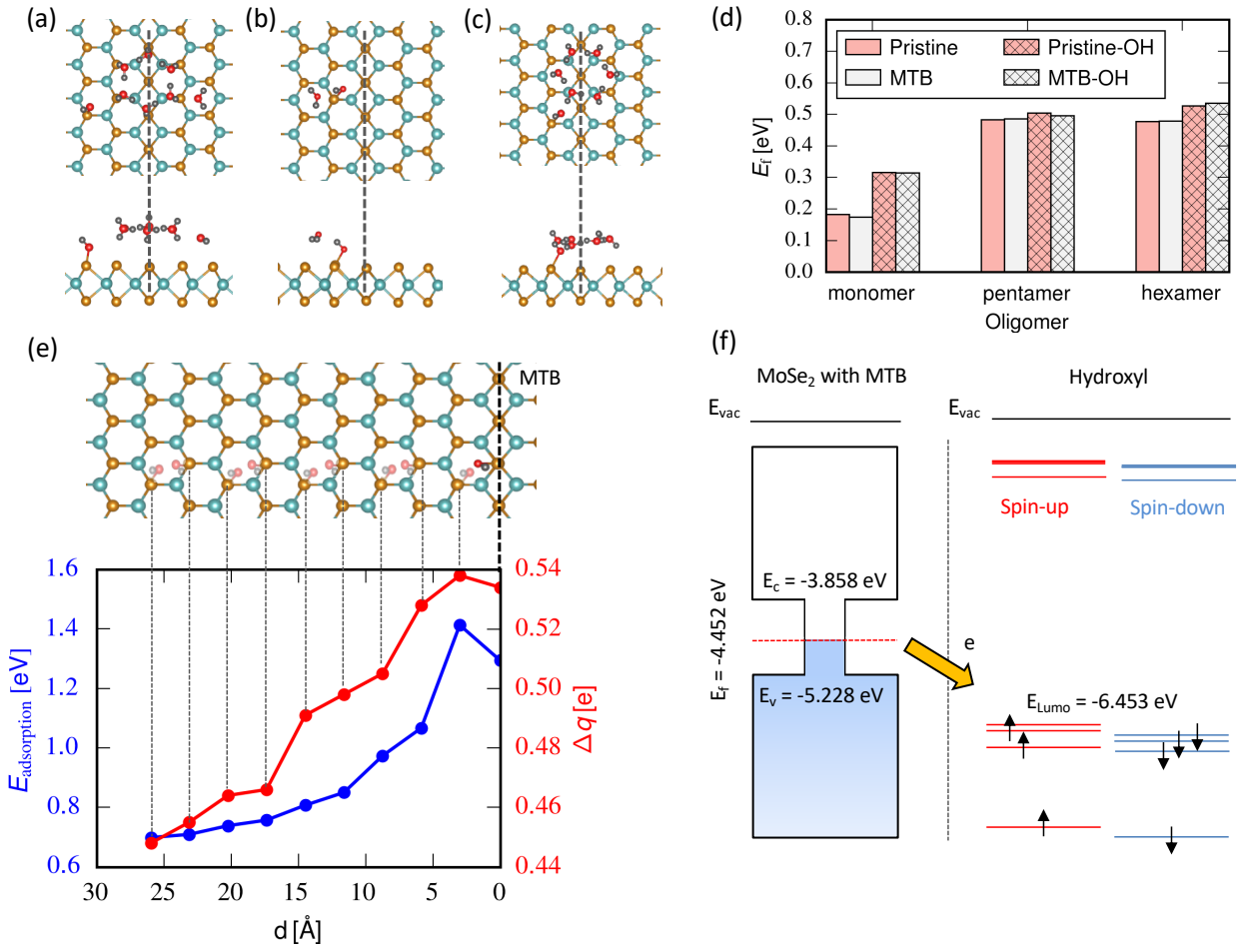

Figure 5: *DFT calculations of water and hydroxyl adsorption on pristine and MTB modified $MoSe_2$. (a-c) Atomic structure of $MoSe_2$ with MTB and adsorbed water molecules, hydroxyl groups and water hexamers attached to the sheet (a) and OH group (b,c). (d) Formation energy of water clusters on top of $MoSe_2$ in the pristine area, next to MTB and OH group. (e) The dependence of adsorption energy of OH group on distance to the MTB. The plot also shows charge transfer from the MTB into the empty molecular orbitals of the hydroxyl group, as schematically illustrated in panel (f).*

Conclusions

The water/TMD interface is critical for ambient and aqueous environments. Weak vdW interactions between the basal plane and water molecules make defects important in enhancing the interactions. Common defects, such as vacancies, exhibit undercoordinated sites that enable stronger adsorption. Here we investigated MTBs that are fully coordinated defect structures, i.e. without dangling bonds, but exhibit metallic defect states within the semiconducting TMDs. While molecular water only adsorbs weakly via vdW interactions at these MTBs, similar to the adsorption on the pristine basal plane, our DFT calculations show that OH- and H- radicals adsorb much stronger on these defects than on pristine $MoSe_2$. This difference is attributed to charge transfer from the metallic defect states to the radicals. These bonded radicals further enhance molecular water adsorption by intermolecular interactions. Thus, the functionalization of MTBs with OH-groups gives rise to the decoration of the MTBs with water and the formation of nanoscopic water network decorating the MTBs. While for water adsorption additional 'anchor groups' are required, in general molecules with appropriate energy levels that enable charge transfer from the MTBs to adsorbate should experience stronger adsorption on the MTBs and thus decorate these line defects. On the other hand, this study also showed that undercoordination of defects is not the only deciding factor to enhance the adsorption of OH- or H- radicals but that appropriate design of band gap states alone can enhance their adsorption. Such defects without dangling bonds but band gap states could be for example substitutional metal dopants and thus provide an approach to design chemical properties of TMDs other than

formation of undercoordinated sites, which so far has been discussed as the main route to enhance chemical activity in applications such as hydrogen evolution electrocatalysis.

Methods:

Sample preparation: *The $MoSe_2$ monolayer islands were grown on freshly cleaved HOPG substrates. Prior to growth the HOPG substrates were outgassed at 400 °C for 6 h. The films were grown at a substrate temperature of 300 °C by co-deposition of Mo and Se from an e-beam evaporator and a hot-wall Se-cracker source, respectively. After growth, the samples are transferred from the growth chamber to a dedicated low temperature scanning tunneling microscope in a vacuum suitcase, keeping the sample in a vacuum better than 10^{-8} Torr.*

Water exposure: *Prior to water exposure the samples were briefly annealed to 200 °C for 40 min to desorb any impurities that may have adsorbed during the sample transfer. Subsequently samples were cooled down in the STM. The STM is a commercial low temperature STM cooled with a closed liquid He-cycle. The sample temperature was close to 20 K for water adsorption and imaging. High purity water was filled into a vacuum sealed quartz tube that was connected to the UHV chamber through a precision leak valve. Prior to dosing, the water was further purified by several freeze-pump cycles. The water was dosed through a stainless-steel tube directed at an opening in the heat shield directly onto the sample, with the STM-tip withdrawn. The water exposure was estimated from a pressure rise in the vacuum chamber and was also monitored with a quadrupole mass spectrometer.*

STM characterization: *Unless otherwise stated the STM images were acquired at 20 K. Electrochemically etched tungsten tips were used.*

Computational: All calculations were carried out using the code VASP.[49,50] *We used generalized gradient approximation with the Perdew-Burke-Ernzerhof (PBE) parametrization[51] for the exchange-correlation (XC) functional and PAW approach[52] to deal with the core electrons. vdW interaction was accounted for using the Grimme approach[53] and the Tkatchenko-Scheffler (TS) scheme[54]. The system was modelled as a ribbon composed from 588 Mo and Se atoms with the MTB in the middle. The vacuum of 15 Å was added above the sheet and also at the edges of the ribbon. As temperature in the experiment was low, and because we were primarily interested in the changes in adsorption energies with the relative position of the species with regard to the*

MTB, he entropic contributions to the Gibbs free energy as well as zero-point energy corrections were not accounted for. The charge transfer upon adsorption of an OH group on $MoSe_2$ monolayer was calculated by integrating the difference between the charge densities of the combined and corresponding isolated systems (for the same geometry) over semi-infinite space with a border being the plane parallel to the monolayer and passing through the middle of the Se-O bond.

Acknowledgement: *Financial support from the National Science Foundation under award NSF-CHE 1801199 is acknowledged. A.V. K. acknowledges financial support from the DFG, project KR 4866/2-1. The authors thank the HZDR computing center, PRACE (HLRS, Stuttgart, Germany, Project ID: 2018184458), and TU Dresden Cluster "Taurus" for generous grants of CPU time.*

References:

1 Thiel, P. A.; Madey, T. E. The Interaction of Water with Solid Surfaces: Fundamental Aspects. *Surf. Sci. Rep.* **1987**, *7*, 211–385.

2 Henderson, M. A. The Interaction of Water with Solid Surfaces: Fundamental Aspects Revisited. *Surf. Sci. Rep.* 2002, *46*, 1–308.

3 Hodgson, A.; Haq, S. Water Adsorption and the Wetting of Metal Surfaces. *Surf. Sci. Rep.* 2009; *64*, 381–451.

4 Verdaguer, A.; Sacha, G. M.; Bluhm, H.; Salmeron, M. Molecular Structure of Water at Interfaces: Wetting at the Nanometer Scale. *Chem. Rev.* **2006**, *106*, 1478–1510.

5 Michaelides, A.; Morgenstern, K. Ice Nanoclusters at Hydrophobic Metal Surfaces. *Nat. Mater.* **2007**, *6*, 597–601.

6 Carrasco, J.; Michaelides, A.; Forster, M.; Haq, S.; Raval, R.; Hodgson, A. A One-Dimensional Ice Structure Built from Pentagons. *Nat. Mater.* **2009**, *8*, 427–431.

7 Guo, J.; Meng, X.; Chen, J.; Peng, J.; Sheng,J.; Li, X.-Z.; Xu, L.; Shi, J.-R.; Wang, E.; Jiang, Y. Real-Space Imaging of Interfacial Water with Submolecular Resolution. *Nat. Mater.* **2014**, *13*, 184–189.

8 Meyer, B.; Marx, D.; Dulub, O.; Diebold, U.; Kunat, M.; Langenberg, D.; Wöll, C. Partial Dissociation of Water Leads to Stable Superstructures on the Surface of Zinc Oxide. *Angew. Chem. Int. Ed.* **2004**, *43*, 6641-6645.

9 Cabrera-Sanfelix, P.; Fernández-Serra, M. V.; Arnau, A.; Sánchez-Portal, D. Substrate-Induced Cooperative Effects in Water Adsorption from Density Functional Calculations. *Phys. Rev. B* **2010**, *82*, 125432.

10 Guevara-Vela, J.M.; Romero-Montalvo, E.; Gómez, V.A.M.; Chávez-Calvillo, R.; García-Revilla, M.; Francisco, E.; Pendás, Á.M.; Rocha-Rinza, T. Hydrogen Bond Cooperativity and Anticooperativity within the Water Hexamer. *Phys. Chem. Chem. Phys.* **2016**, *18*, 19557-19566.

11 Salmeron, M.; Bluhm, H.; Tatarkhanov, M.; Ketteler, G.; Shimizu, T.K.; Mugarza, A.; Deng, X.; Herranz, T.; Yamamoto, S.; Nilsson, A. Water Growth on Metals and Oxides: Binding, Dissociation and Role of Hydroxyl Groups. *Faraday Discuss.* **2009**, *141*, 221-229.

12 Halwidl, D.; Stöger, B.; Mayr-Schmölzer, W.; Pavelec, J.; Fobes, D.; Peng, J.; Mao, Z.; Parkinson, G.S.; Schmid, M.; Mittendorfer, F.; Redinger, J.; Diebold, U. Adsorption of Water at the SrO Surface of Ruthenates. *Nat. Mater.* **2016**, *15*, 450–455.

13 Hussain, H.; Ahmed, M.H.M.; Torrelles, X.; Grinter, D.C.; Cabailh, G.; Bikondoa, O.; Nicklin, C.; Aschauer, U.; Lindsay, R.; Thornton, G. Water-Induced Reversal of the TiO_2(011)-(2 × 1) Surface Reconstruction: Observed with in Situ Surface X-ray Diffraction. *J. Phys. Chem. C* **2019**, *123*, 13545−13550.

14 Hennessy, D.C.; Pierce, M.; Chang, K.C.; Takakusagi, S.; You H.; Uosaki, K. Hydrophilicity transition of the clean rutile TiO_2 (110) surface. *Electrochim. Acta* **2008**, *53*, 6173-6177.

15 Treacy, J.P.W.; Hussain,H.; Torrelles, X.; Cabailh, G.; Bikondoa, O.; Nicklin, C.; Thornton, G.; Lindsay R. Structure of a Superhydrophilic Surface: Wet Chemically Prepared Rutile-TiO_2(110)(1 × 1). J*. Phys. Chem. C* **2019**, *123*, 8463–8468.

16 Merte, L.R.; Bechstein, R.; Peng, G.; Rieboldt, F.; Farberow, C.A.; Zeuthen, H.; Knudsen, J.; Lægsgaard, E.; Wendt, S.; Mavrikakis, M.; Besenbacher, F. Water Clustering on Nanostructured Iron Oxide Films. *Nat. Commun.* **2014**, *5*, 4193.

17 Levita, G.; Restuccia, P.; Righi, M.C. Graphene and MoS_2 Interacting with Water: A Comparison by a*b Initio* Calculations. *Carbon* **2016**, *107*, 878-884.

18 Ferreira, F.; Carvalho, A.; Moura, Í.J.M.; Coutinho, J.; Ribeiro, R.M. Adsorption of H_2, O_2, H_2O, OH and H on monolayer MoS_2. *J. Phys.: Condens. Matter* **2018**, *30*, 035003.

19 Ghuman, K.K.; Yadav, S.; Singh, C.V. Adsorption and Dissociation of H_2O on Monolayered MoS_2 Edges: Energetics and Mechanism from *ab Initio* Simulations. *J. Phys. Chem. C* **2015**, *119*, 6518–6529.

20 Cabrera Sanfelix, P.; Holloway, S.; Kolasinski, K.W.; Darling, G.R. The Structure of Water on the (0 0 0 1) Surface of Graphite. *Surf. Sci.* **2003**, *532–535*, 166–172.

21 Standop, S.; Michely, T.; Busse, C. H_2O on Graphene/Ir(111): A Periodic Array of Frozen Droplets. *J. Phys. Chem. C* **2015**, *119*, 1418−1423.

22 Ma, H.; Brugger, T.; Berner, S.; Ding, Y.; Iannuzzi, M.; Hutter, J.; Osterwalder, J.; Greber, T. Nano-Ice on Boron Nitride Nanomesh: Accessing Proton Disorder. *Chem. Phys. Chem.* **2010**, *11*, 399 -403.

23 Uhlig, M.R.; Martin-Jimenez, D.; Garcia, R. Atomic-Scale Mapping of Hydrophobic Layers on Graphene and Few-Layer MoS_2 and WSe_2 in Water. *Nat. Commun.* **2019**, *10*, 2606.

24 Voiry, D.; Yang, J.; Chhowalla, M. Recent Strategies for Improving the Catalytic Activity of 2D TMD Nanosheets Toward the Hydrogen Evolution Reaction. *Adv. Mater.* **2016**, *28*, 6197-6206.

25 Kibsgaard, J.; Chen, Z.; Reinecke, B. N.; Jaramillo, T. F. Engineering the Surface Structure of MoS_2 to Preferentially Expose Active Edge Sites for Electrocatalysis. *Nat. Mater.* **2012**, *11*, 963-969.

26 Li, H.; Tsai, C.; Koh, A.L.; Cai, L.; Contryman, A.W.; Fragapane, A.H.; Zhao, J.; Han, H.S.; Manoharan, H.C.; Abild-Pedersen, F.; Nørskov, J.K.; Zheng, X. Activating and Optimizing MoS_2 Basal Planes for Hydrogen Evolution Through the Formation of Strained Sulphur Vacancies. *Nat. Mater.* **2016**, *15*, 48-53.

27 He, Y.; Tang, P.; Hu, Z.; He, Q.; Zhu, C.; Wang, L.; Zeng, Q.; Golani, P.; Gao, G.; Fu, W.; *et al.* Engineering Grain Boundaries at the 2D Limit for the Hydrogen Evolution Reaction. *Nat. Commun.* **2020**, *11*, 57.

28 Kosmala, T.; Diaz, H.C.; Komsa,H.-P.; Ma, Y.; Krasheninnikov, A.V.; Batzill, M.; Agnoli, S. Metallic Twin Boundaries Boost the Hydrogen Evolution Reaction on the Basal Plane of Molybdenum Selenotellurides. *Adv. Energ. Mater.* **2018**, *8*, 1800031.

29 Komsa, H.-P.; Krasheninnikov, A.V. Engineering the Electronic Properties of Two-Dimensional Transition Metal Dichalcogenides by Introducing Mirror Twin Boundaries. *Adv. Electr. Mater.* **2017**, *3*, 1600468.

30 Lehtinen, O.; Komsa, H.-P.; Pulkin, A.; Whitwick, M.B.; Chen, M.-W.; Lehnert, T.; Mohn, M.J.; Yazyev, O.V.; Kis, A.; Kaiser, U.; Krasheninnikov, A.V. Atomic Scale Microstructure and Properties of Se-Deficient Two-Dimensional $MoSe_2$. *ACS Nano* **2015**, *9*, 3274–3283.

31 M Batzill. Mirror Twin Grain Boundaries in Molybdenum Dichalcogenides. *J. Physics: Condens. Matter* **2018**, *30*, 493001.

32 Coelho, P.M.; Komsa, H.-P.; Diaz, H.C.; Ma, Y.; Krasheninnikov, A.V.; Batzill, M. Post-Synthesis Modifications of Two-Dimensional $MoSe_2$ or $MoTe_2$ by Incorporation of Excess Metal Atoms into the Crystal Structure. *ACS Nano* **2018,** *12*, 3975-3984.

33 Lin, X.; Lu, J.C.; Shao, Y.; Zhang, Y.Y.; Wu, X.; Pan, J.B.; Gao, L.; Zhu, S.Y.; Qian, K.; Zhang, Y. F.; *et al.* Intrinsically Patterned Two-Dimensional Materials for Selective Adsorption of Molecules and Nanoclusters. *Nat. Mater.* **2017**, *16*, 717–721.

34 Ma, Y.; Diaz, H.C.; Avila, J.; Chen, C.; Kalappattil, V.; Das, R.; Phan, M.-H.; Čadež, T.; Carmelo, J.M.P.; Asensio, M.C.; Batzill, M. Angle Resolved Photoemission Spectroscopy Reveals Spin Charge Separation in Metallic $MoSe_2$ Grain Boundary. *Nat. Commun.* **2017**, *8*, 14231.

35 Ma, Y.; Kolekar, S.; Diaz, H.C.; Aprojanz, J.; Miccoli, I.; Tegenkamp, C.; Batzill, M. Metallic Twin Grain Boundaries Embedded in $MoSe_2$ Monolayers Grown by Molecular Beam Epitaxy. *ACS Nano* **2017**, *11*, 5130-5139.

36 Jolie, W.; Murray, C.; Weiß, P.S.; Hall, J.; Portner, F.; Atodiresei, N.; Krasheninnikov, A.V.; Busse, C.; Komsa, H.P.; Rosch, A.; Michely, T. Tomonaga-Luttinger Liquid in a Box: Electrons Confined within MoS_2 Mirror-Twin Boundaries. *Phys. Rev. X* **2019**, *9*, 011055 (2019).

37 Liu, H.; Jiao, L.; Yang, F.; Cai, Y.; Wu, X.; Ho, W.; Gao, C.; Jia, J.; Wang, N.; Fan, H.; Yao, W.; Xie, M. Dense Network of One-Dimensional Midgap Metallic Modes in Monolayer $MoSe_2$ and Their Spatial Undulations. *Phys. Rev. Lett.* **2014**, *113*, 066105.

38 Barja, S.; Wickenburg, S.; Liu, Z.-F.; Zhang, Y.; Ryu, H.; Ugeda, M.M.; Hussain, Z.; Shen, Z.-X.; Mo, S.-K.; Wong, E.; Salmeron, M.B.; Wang, F.; Crommie, M.F.; Ogletree, D.F.; Neaton, J.B.; Weber-Bargioni, A. Charge Density Wave Order in 1D Mirror Twin Boundaries of Single-Layer $MoSe_2$. *Nat. Phys.* (2016), *12*, 751–756.

39 He, X.; Zhang, L.; Chua, R.; Wong, P.K.J.; Arramel, A.; Feng, Y.P.; Wang, S.J.; Chi, D.; Yang, M.; Huang, Y.L.; Wee, A.T.S. Selective Self-Assembly of 2,3-Diaminophenazine Molecules on $MoSe_2$ Mirror Twin Boundaries. *Nat. Commun.* **2019**, *10*, 2847.

40 Levita, G.; Restuccia, P.; Righi M.C. Graphene and MoS_2 Interacting with Water: A Comparison by *ab Initio* Calculations. *Carbon* **2016**, *107*, 878-884.

41 Michaelides, A. Density Functional Theory Simulations of Water–Metal Interfaces: Waltzing Waters, a Novel 2D Ice Phase, and More. *Applied Physics A* **2006**, 85, 415–425.

42 Chepkasov, I.V.; Ghorbani-Asla, M.; Popov, Z.I.; Smet, J. H.; Krasheninnikov, A.V. Alkali metals inside bi-layer graphene and MoS_2: Insights from first-principles calculations. *Nano Energy* **2020**, *75*, 104927.

43 Ataca, C.; Ciraci, S. Dissociation of H_2O at the Vacancies of Single-Layer MoS_2. *Phys. Rev. B* **2012**, *85*, 195410.

44 Hao, Y.; Gong, P.L.; Xu, L.-C.; Pu, J.; Wang, L.; Huang, L.-F. Contrasting Oxygen Reduction Reactions on Zero- and One-Dimensional Defects of MoS_2 for Versatile Applications. *ACS Appl. Mater. Interf.* **2019**, *11*, 46327-46336.

45 Shu, H.; Zhou, D.; Li, F.; Cao, D.; Chen, X. Defect Engineering in $MoSe_2$ for the Hydrogen Evolution Reaction: From Point Defects to Edges. *ACS Appl. Mater. Interf.* **2017**, *9*, 42688–42698.

46 Tsai, C.; Chan, K.; Abild-Pedersen, F.; Nørskov, J.K. Active Edge Sites in $MoSe_2$ and WSe_2 Catalysts for the Hydrogen Evolution Reaction: A Density Functional Study. *Phys. Chem. Chem. Phys.* **2014**, *16*, 13156-13164.

47 Levita G., Restuccia P., Righi M. Graphene and MoS_2 Interacting with Water: A Comparison by *ab Initio* Calculations. *Carbon* **2016**, *107,* 878-884.

48 Ghuman, K.K.; Yadav, S.; Singh, C.V. Adsorption and Dissociation of H_2O on Monolayered MoS_2 Edges: Energetics and Mechanism from *ab Initio* Simulations. *J. Phys. Chem. C* **2015**, *119*, 6518-6529.

49 Kresse, G.; Hafner, J. *Ab Initio* Molecular Dynamics for Liquid Metals. *Phys. Rev. B* **1993**, *47*, 558–561.

50 Kresse, G.; Furthmüller, J. Efficiency of *ab Initio* Total Energy Calculations for Metals and Semiconductors Using a Plane-Wave Basis Set. *Comput. Mater. Sci.* **1996**, *6*, 15-50.

51 Perdew, J. P.; Burke, K.; Ernzerhof, M. Generalized Gradient Approximation Made Simple. *Phys. Rev. Lett.* **1996**, 77, 3865-3868.

52 Blöchl, P. E. Projector Augmented-wave Method. *Phys. Rev. B* **1994**, *50*, 17953-17979.

53 Grimme, S. Semiempirical GGA-Type Density Functional Constructed with a Long-Range Dispersion Correction. *J. Comput. Chem.* **2006**, *27*, 1787-1799.

54 Tkatchenko, A.; Scheffler, M. Accurate Molecular Van Der Waals Interactions from Ground-State Electron Density and Free-Atom Reference Data. *Phys. Rev. Lett.* **2009**, *102*, 073005.